Low friction and wear resistant coatings

Carvalho, Nuno Jorge Marcolino

6

MECHANICAL PROPERTIES OF TiN AND TiN/(Ti,Al)N MULTILAYERS

6.1 INTRODUCTION

Physical vapour deposited (PVD) TiN and TiN/(Ti,Al)N multilayers are currently used in tooling applications achieving an increase in lifetime of up to ten times.[1,2] The wear resistance is attributed to their mechanical properties (e.g. high hardness) and chemical inertness. The wear behaviour of these hard ceramic coatings on tool and machine elements depends also on the adhesion to the substrate and the ability to prevent crack initiation and propagation. The mechanical properties of materials on the micron and sub-micrometer scale are often investigated by indentation hardness testing.[3,4] The recent development of nanoindentation instruments that continuously measure the contact stiffness as the indenter is driven into the sample, leads to a more accurate determination of the mechanical response of thin films.

In this chapter, the mechanical behaviour, and ultimately the properties of the coatings are probed by going down on the length-scales so that changes as a function of decreasing contact load – and increasing coating importance – can be investigated. Vickers hardness tests are performed to evaluate the performance of the coated systems when submitted to high loads, and nanoindentation to tackle the properties at loads where the coating should dominate.

The coated systems were also submitted to a rolling contact test technique to obtain some clarification of the mechanism of interfacial failure and consequently the coating adhesion. This mechanism can be characterised by the understanding of the relationship between surface roughness, surface hardness, contact stress and fatigue durability. Moreover, the understanding of different types of fatigue crack growth mode can give an insight of the bonding between coating and the substrate. The advantage of this technique over scratch tests is that the critical load is a sensitive measure of the bonding conditions at the coating-substrate interface and it remains insensitive to the testing conditions.[5] Scanning electron microscopy (SEM) has been the main technique utilised in this chapter to study the coated systems.

6.2 COATED SYSTEMS AND EXPERIMENTAL METHODS

The TiN and TiN/(Ti,Al)N multilayers were deposited onto substrates with several combinations of hardness and roughness to investigate their influence on the composite system. Knowledge of the role the substrate condition play with respect to the adhesion strength of hard coatings is invaluable in order to predict the system performance in a real contact situation. Table 6.1 summarises the relevant details of the coating-substrate systems.

The indentations were performed at room temperature on as–deposited coatings and substrate materials with mirror-finishing surfaces. Vickers indentations were carried out using a Leitz microhardness tester with loads ranging from 25 to 500 gf (245 mN to 4.9 N). To ensure that the deformation introduced by earlier indentations did not influence the following ones, they were spaced 300 μm apart. For all hardness calculations, 7 diagonals were measured at each load to produce a mean diagonal and a standard deviation. The hardness calculated from the latter was plotted *versus* the load for each sample.

Conventional load-displacement-time indentation cycles (nanoindentation) were performed under both load and displacement control to peak loads ranging from 5 mN to 500 mN. Indentations to obtain hardness and modulus values were performed with the continuous stiffness module (CSM), to a large

Table 6.1 *Combination of coating-substrate composites investigated.*

Coating	Substrate material	Substrate hardness HV [GPa]	Substrate pre-treatment	Substrate roughness R_a [μm]
TiN	Cold work steel (AISI D2)	5.0	Polished	0.03
TiN	Cold work steel (AISI D2)	6.8	Polished	0.03; 0.15
TiN	Cold work steel (AISI D2)	6.8	Ground	0.10
TiN	High speed steel (Vanadis 30)	8.8	Polished	0.03; 0.10; 0.25
TiN/(Ti,Al)N	Cold work steel (AISI D2)	6.8	Polished	0.03
TiN/(Ti,Al)N	Cold work steel (AISI D2)	6.8	Ground	0.10
TiN/(Ti,Al)N	High speed steel (Vanadis 30)	8.8	Polished	0.05; 0.11

pre-determined maximum load of 500 mN. For each experiment the CSM imposed a 1 nm oscillation at 45 Hz on the loading curves. The measurements were repeated twenty times and were all performed using the constant loading rate (*dP/P*) sequence. This procedure permits large numbers of data points to be accumulated in the low-load segment of each data set, something particularly useful when undertaking experiments on coated systems.[6] The value of *dP/P* was 0.05. Holding segments at full load and 70% unloading were used to allow for compensation of creep and any thermal drift, respectively. The data were

analysed using standard Nano Instruments software to generate data for load, displacement, and stiffness. Then, load-displacement curves were plotted. Sample hardness and modulus as a function of load were also calculated.

The experimental procedure for rolling contact fatigue tests was similar to the one employed with the WC/C multilayers (see chapter 4). However, in this case, systems having the cold work steel substrate (AISI D2), the maximum contact stress of the coated systems produced by an applied load ranging from 0.4 to 1.2 kN was between 4.2 and 5.4 GPa. The maximum equivalent stress was also in the regime of elastic-plastic deformation of the substrate. In systems with high speed steel substrate (Vanadis 30), a normal load of 1050 N corresponded to a maximum contact stress of 6.4 GPa.

6.3 VICKERS MICROHARDNESS

Composite and substrate Vickers hardness values were measured for as-deposited TiN coating onto two tool steel materials with different hardness. Figure 6.1 displays the Vickers hardness values *versus* indentation depth (theoretically given by the geometrical relation $D \approx d/7$, see §2.4.1). The Vickers hardness, also termed conventional hardness, is calculated from the final displacement after complete unloading. Although, it may be a useful means of characterising the mechanical response of plasticity-dominated solids, e.g. the substrates, it is an ambiguous parameter for materials with mixed elastic/plastic behaviour as the coated systems investigated. However, it is still a practical and straightforward method of assessing the behaviour of coated systems under a load range not available by nanoindentation techniques. The curves were fitted to the experimental points by a power law.

The hardness values obtained for substrate materials display a slight dependence on load at small indentations sizes. This phenomenon is often termed as the indentation size effect (ISE). It is probably related to the increased importance of elastic deformation at small sizes together with the marked increase in difficulty of initiating plastic flow in small volumes of material.[7] The data from the composite systems at displacements similar to the coating thickness shows that the coating still enhances the hardness, as is indicated by

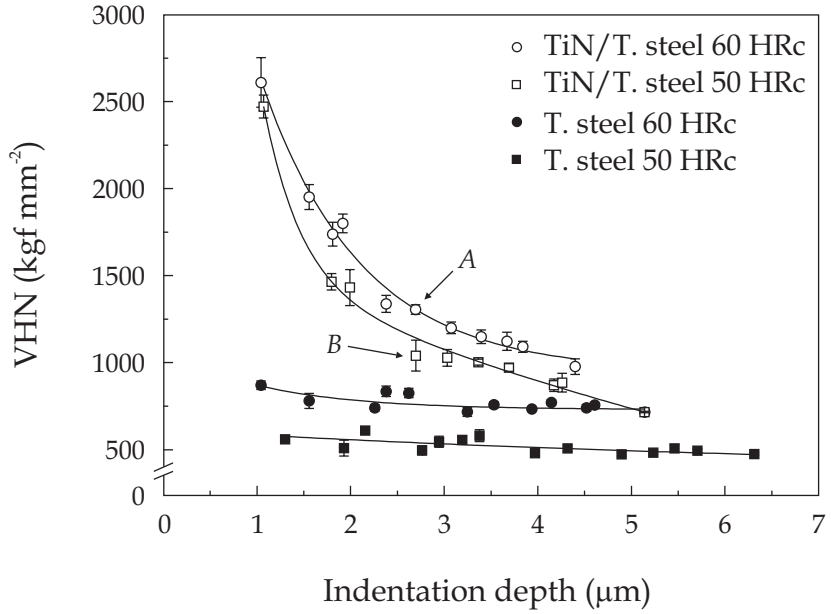

Figure 6.1 *Mean Vickers hardness values vs indentation depth of the composite materials and bare substrates. Indentation depths A and B correspond to loads of 250 gf and 200 gf on composites with a substrate of 60 HRc (VHN 697 kgf mm^{-2}) and 50 HRc (VHN 513 kgf mm^{-2}), respectively.*

higher composite values compared to the substrates alone. The composite systems exhibit considerable increase in hardness with decreasing indentation depth. This increase reflects the increasing importance of the harder coating in the determination of system properties for smaller depths and a markedly ISE dependence. Nevertheless, the substrate still plays a role, as can be seen by the lower hardness value obtained from system with a softer substrate. The large scatter obtained for lower loads is related to the inaccuracy of measuring the residual indentation diameter in the SEM.

An example of a rather perfect indentation impression on substrate material is shown in figure 6.2a. The geometry of the indentation does not change during the load range applied due to the low percentage of elastic recovery of the material. Based on experimental observations, two different "geometries" of indentations on composite materials can be identified and correlated to the curve of the hardness *versus* indentation depth. The first, formed at loads

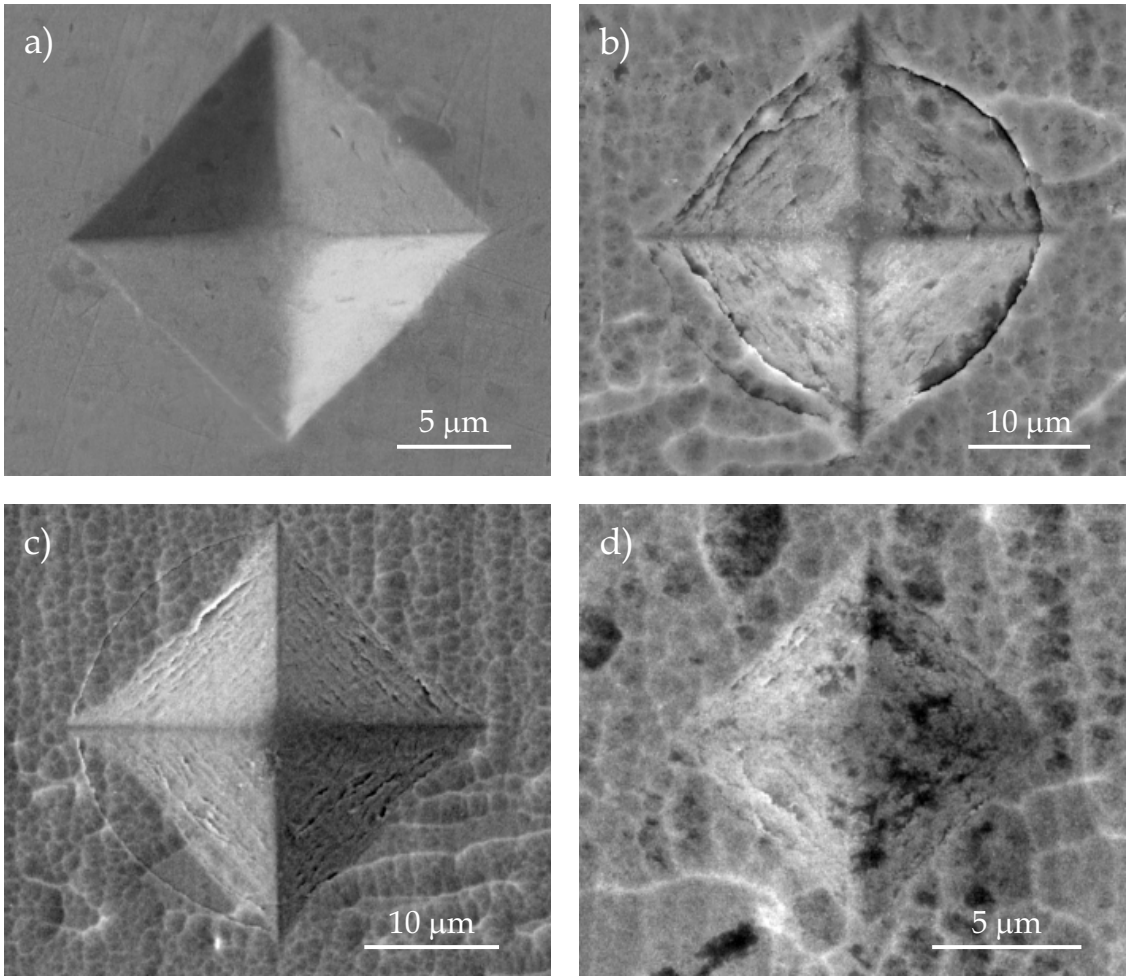

Figure 6.2 *SEM micrographs showing Vickers hardness impressions:* (a) *200 gf on tool steel substrate with 60 HRc;* (b) *500 gf on TiN coated system with a substrate of 50 HRc;* (c) *500gf on TiN coated system with a substrate of 60 HRc;* (d) *125 gf on TiN coated system with a substrate of 50 HRc .*

beyond *A* and *B* have a distinctly concave impression with cracks in the surrounding surface. At higher loads the composite material with the softer substrate was deformed by a fully developed crack around the rim of the impression (figure 6.2b), while the composite material with harder substrate is deformed only by a half-circle (figure 6.2c). It is interesting to note that the crack initiation around the rim of the impression for the two composites materials is observed at different loads, but at approximately the same indentation depth of

2.7 μm. The second regime is formed at loads below *A* and *B*. The contact areas have slighter concave impression sides with parallel cracks inside the indented region, but have no deformation of the surface outside (figure 6.2d).

These two regimes can be explained by considering that for higher indentation depths the coating is unable to follow the flexure and plastic deformation of the substrate created by the large surface area of the pyramidal indentation. Therefore a through-thickness circular crack is developed around the rim on the impression. Figure 6.2b, shows that the coating has not only cracked around the rim, but also that the crack has been pulled open by plastic flow of the underlying substrate. For more shallow surface areas, the indenter only bents and stretches the coating into the substrate. This causes tensile stresses to develop on the coating around the edges of the indentation creating an array of nested parallel cracks within the indentation profile.[4] Thus, those cracks reveal the successive positions of the indentation edges. The high fracture toughness of the coated systems is illustrated by the absence of surface radial cracks emanating at the indentation corners.

6.4 NANOINDENTATION RESPONSE

The load-displacement curves of tool steel substrates are shown in Figure 6.3a. The behaviour is typical of a ductile, plastic material, i.e. like most metals. The loading curve is approximately parabolic and the unloading segment is very abrupt. This indicates that the elastic strains during indentation are small compared with the plastic strains, resulting in a little elastic recovery of the indentation depth. The plastic strains are evident even at low loads, as is perceived by the percentage of elastic recovery during unloading for both materials, being 25% ± 4% for the 50 HRc substrate and 38% ± 7% for the 60 HRc substrate.

Evaluating the response of coated systems with respect to the substrate enables one to highlight the properties of the coating itself. Figure 6.3b shows typical load-displacements curves of both systems. In contrast to the substrates, the load-displacement curves of the coated systems exhibit increased amounts of elastic recovery on unloading. It establishes that a higher proportion of the

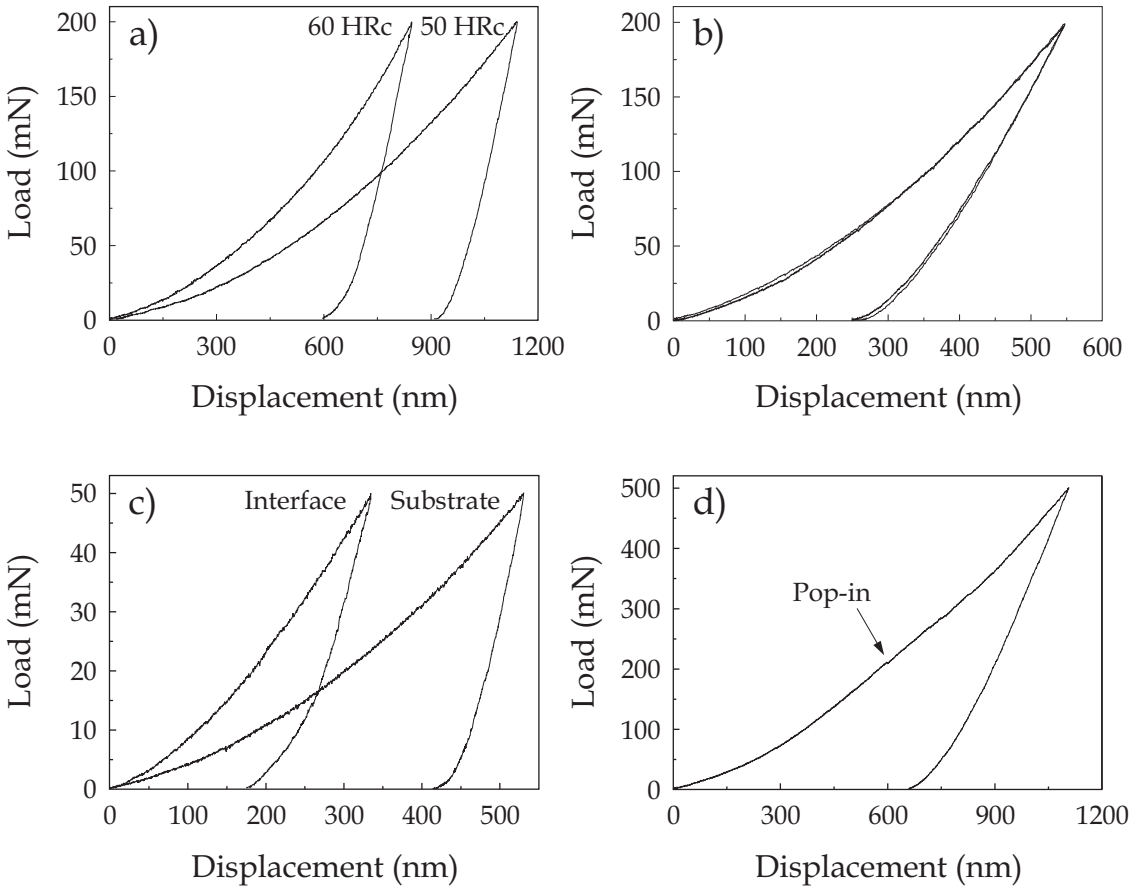

Figure 6.3 *Nanoindentation load-displacement curves showing different characteristic features observed in the response of substrates and TiN coated systems:* (a) *behaviour of both substrates for peak load of 200 mN;* (b) *overlapping curves of the TiN coated systems with two different substrates (50 HRc and 60 HRc) at peak load of 200 mN;* (c) *load-displacement curves of the substrate and "interfacial" nanoindentations at 50 mN peak load;* (d) *load-displacement curve of TiN coated system exhibiting a discrete displacement discontinuity "pop-in" produced by crack propagation in the coating.*

deformation is accommodated elastically. When the both coated systems are compared at higher peak loads (note the overall indenter displacement is still small compared with the coating thickness) the difference in percentage of elastic recovery is more pronounced. Also, the fact that the system with the softer substrate displays a smaller percentage of elastic recovery, leads to the conclusion that the relative contribution of the coating to the system response is

less. On the other hand, at low peak loads the influence of the substrate is very reduced, as can be seen by the similar maximum displacement of both curves. Thus, evidencing that at this contact load regime the response of the system depends primarily on the ability of the coating to support the load.

The influence of the interfacial region, and hence an indication of the interfacial adhesion is displayed in figure 6.3c. It shows the load-displacement curve of a nanoindentation at the interface by cross-sectioning the coated system, and for comparison the load-displacement curve of the substrate. The corresponding indentation impressions are presented by SEM micrographs in figure 6.4. For the same peak load, the "interfacial" load-displacement curve exhibits a smaller indenter penetration than the substrate. Also, at the final stages of unloading, the interfacial curve becomes less steep, indicating a larger fraction of elastic recovery. Thus, even when nanoindentation is performed only with one side of the indenter penetrating the coating, it is possible to see the influence of the coating on the system.

The load-displacement curve in figure 6.3d contains a small step or "pop-in". When the loading curve presents such sudden forward displacement without any increase in applied load, it is an indication that the coating might have cracked, relaxing locally any membrane or residual stresses.[8,9] However, significant membrane stresses are still retained in the coating and the unloading curve is quite distinct from that of the substrate alone. The observation of cracks only at the maximum load, i.e. not at lower applied stresses, indicates that during bending the combination of elastic flexure of the coating, plastic yielding of the substrate, and any membrane stresses generated in the coating can still support the indentation load.[10,11] Due to technical problems it was not possible to perform a comprehensive investigation of the TiN/(Ti,Al)N coated systems response to nanoindentation. However, the hardness and Young's modulus were measured, allowing a discussion of these mechanical properties from both systems.

Nanoindentation hardness values for TiN and TiN/(Ti,Al)N multilayer coated systems are plotted in figure 6.5 as a function of the displacement into the surface. The increase in hardness observed for shallow displacements is thought to result from uncertainties in the tip end-shape calibration, whereas the larger

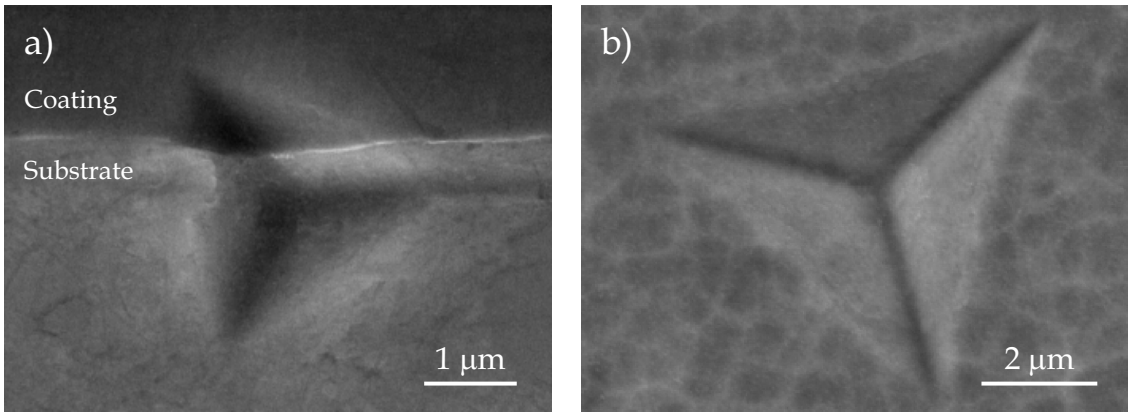

Figure 6.4 *SEM micrographs showing the indentation impression on the TiN coated system:* (a) *50 mN nanoindentation performed on cross-sectional sample at the coating-substrate interface. Note that actually only one of the indenter vertices penetrates the coating;* (b) *200 mN nanoindentation performed on plan-view sample.*

scatter is primarily due to surface roughness of the as-deposited coatings. The results also confirm the assumptions made before about probing the coatings properties at displacements lower than its thickness. For penetration depths in the order of few hundred nanometers the influence of the substrate to the composite hardness values is much reduced. This is clear when comparing the values from TiN onto different substrate hardness. The hardness of the multilayers at low displacements is essentially the same as for the homogeneous layer. However, with penetration depth the difference in hardness becomes more pronounced. This enhancement is related to a hardening effect caused by the large number of interfaces parallel to the substrate surface. By assuming that at an indenter penetration of 200 nm the influence of both tip-shape irregularities (the tip radius is 40 – 50 nm) and substrate (penetration depth less than one-tenth of coating thickness) are negligible, it is possible to estimate the coating hardness. Thus, the TiN and the TiN/(Ti,Al)N multilayers have a hardness of the order of 31 GPa.

When the hardness values obtained with the CSM option and Vickers are correlated, it is possible to draw the following conclusions: At displacements corresponding to the coating thickness, the coating basically behaves as a cap

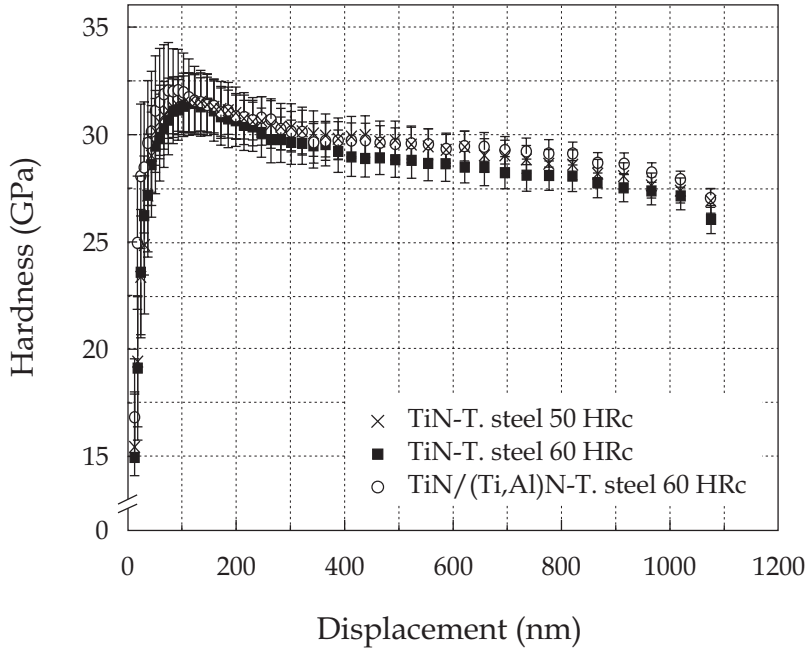

Figure 6.5 *Mean hardness values as a function of the indenter displacement of the homogeneous TiN and the TiN/(Ti,Al)N multilayers onto steel substrates with 50 HRc (5.0 GPa) and 60 HRc (6.8 GPa). The data were derived utilising the continuous stiffness option.*

on the tip of the indenter transmitting the applied load to the substrate; for lower displacements the coating properties commence to come into sight, and at displacements of the order of one-tenth of the coating thickness the influence of substrate hardness is barely detectable.

Figure 6.6 shows the mean effective Young's modulus as a function of indenter displacement for TiN and TiN/(Ti,Al)N multilayer coated systems. The values were also derived from the continuous stiffness measurements. The effective modulus decreases markedly with increasing displacement into the coated system. TiN systems displays values systematically higher than the multilayers counterpart. However, the larger variation at lower displacements is correlated to the difference of Poisson's ratio of each coating. Although this value is not known for the multilayers, it is certainly lower than the one of the homogeneous layer. This reasoning is based on the calculated values of the Poisson's ratio for (Ti,Al)N and TiN (see chapter 5) and the presence of a thick

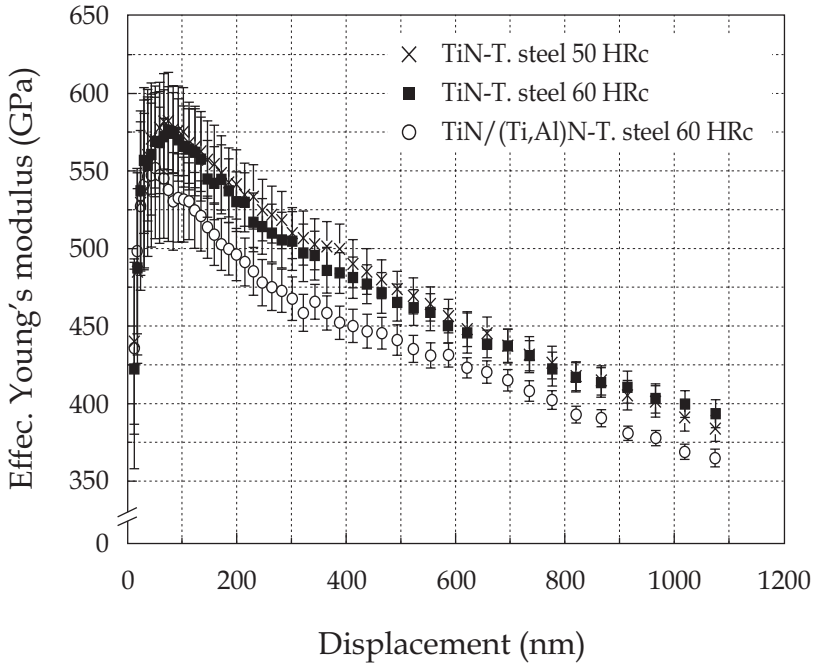

Figure 6.6 *Mean effective Young's modulus values as a function of the indenter displacement of the homogeneous TiN and the TiN/(Ti,Al)N multilayers onto steel substrates with 50 and 60 HRc. The substrate of the systems has a Young's modulus of 210 GPa. The data were derived utilising the continuous stiffness option.*

(Ti,Al)N top layer. With the Poisson's ratio of TiN, it is possible to estimate a Young's modulus of 500 GPa. The value for the multilayer can be estimated, by allowing for a Poisson's ratio a value close to 0.177, to be 480 GPa. These values are within the range of the commonly reported in literature.[12-14]

6.5 ROLLING CONTACT FATIGUE

6.5.1 FATIGUE LIFETIME

The first tests were run on bare substrates under a maximum contact stress of 4.1 GPa. It was found that no pitting (surface fatigue) of the bulk material had occurred. Figure 6.7 displays the results from coated systems with dissimilar substrate pre-treatments and surface roughness. It is evident that the fatigue lifetime is influenced by a combination of contact stresses and the state of the

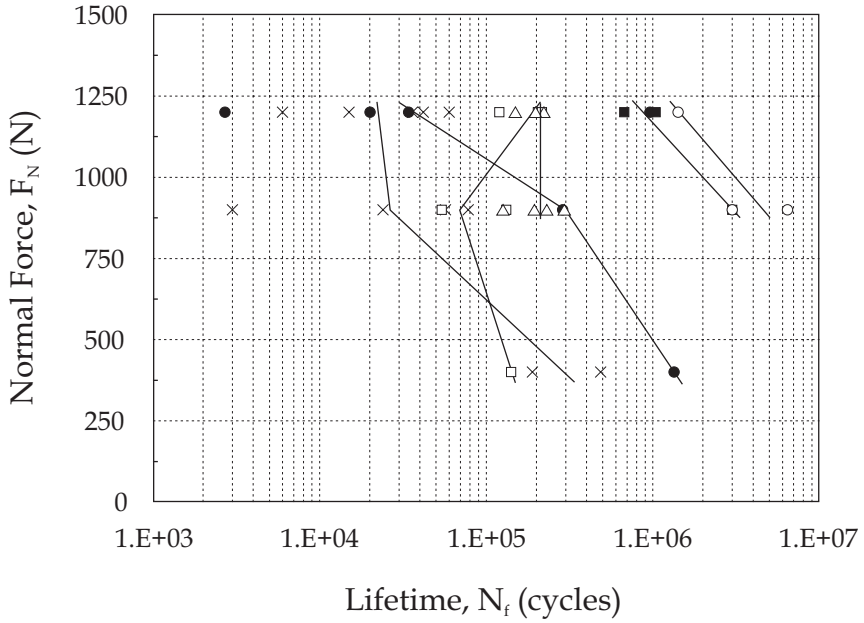

Figure 6.7 *Rolling contact fatigue results of the TiN and the TiN/(Ti,Al)N multilayers onto steel substrates with different pre-treatment and surface roughness. The substrates have a 60 HRc. Results of a system with a substrate of 50 HRc are also presented as reference. The fitting lines are obtained by averaging the lifetime of the tests performed at each normal force. [Key: △ TiN onto polished 50 HRc substrate, R_a=0.03 μm; ● TiN onto polished substrate, R_a=0.03 μm; × TiN onto polished substrate, R_a=0.15 μm; □ TiN onto ground substrate, R_a=0.1 μm; ○ TiN/(Ti,Al)N onto ground substrate, R_a=0.1 μm; ■ TiN/(Ti,Al)N onto polished substrate, R_a=0.03 μm].*

substrate surface. The following trends are observed for TiN coated systems: Especially at lower contact stresses the pre-treatment and the surface roughness, have a large influence on the fatigue lifetime, with the fine polished surface associated with longer life. However, at the highest contact stress the results show a reduced influence; tests performed on systems with a substrate of 60 HRc exhibit a much larger standard deviation than those with a substrate of 50 HRc. The rolling contact fatigue results for TiN/(Ti,Al)N multilayer coated systems demonstrate that there is a slender difference between the ground and polished substrate pre-treatments. This is thought to be related to the high surface roughness of the coatings induced by the TiN droplets (see e chapter 5).

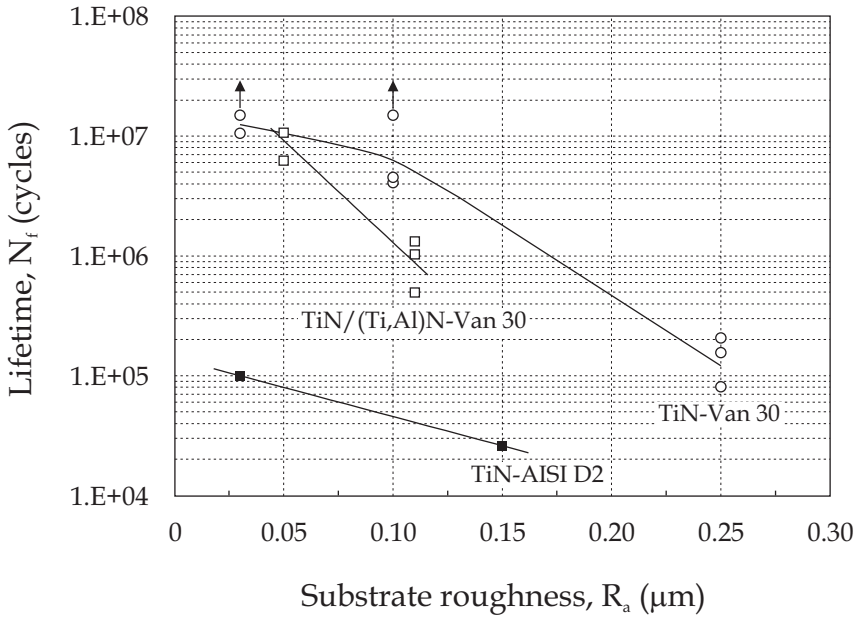

Figure 6.8 *Rolling contact fatigue results of the TiN and the TiN/(Ti,Al)N multilayers onto polished steel substrates. All tests were subjected to a normal force, F_N, of 1050 N. The arrows indicate tests that were automatically stopped when a 500 hours running time was achieved without fatigue failure.*

In order to investigate separately the influence of the substrate roughness on the coated systems fatigue lifetime, a set of tests was performed at a single contact load and on systems with the same polishing pre-treatment. Figure 6.8 presents the results. All systems investigated displayed a reduced fatigue lifetime with increasing substrate roughness. However, the behaviour was less pronounced for the TiN onto cold work steel. This fact is not surprising because the corresponding maximum equivalent stress (due to a 1050 N normal load) is in the elastic-plastic deformation regime. Therefore, as the coating with the surface of the substrate deforms, the stress levels within the coating or at the coating-substrate interface might become higher than the shear strength of the system. This leads to failure of the coated systems by fracture. In systems with a high speed steel substrate, the coating has a higher loading resistance without failure by fracture because of an increased resistance to deflection.[15] Moreover, the maximum equivalent stress created by the normal load is in the elastic

regime. Then, the influence of the substrate roughness is enhanced because it is transmitted to the coating surface. Additionally, the Hertzian contact pressure field might be significantly altered due to the surface roughness.[16]

It has been shown that coating thickness is a key parameter for improving the lifetime in rolling contacts with hard coatings[17-19]. The optimum coating thickness seems to be in the range of 0.1 to 1 μm, because a thin hard coating is more able to deform elastically and to follow the substrate deformation without delamination. Also, as revealed in chapter 5, the thinner coatings contain higher compressive stresses which might compensate the tensile stresses generated upon substrate deformation. On the other hand, thicker coatings have an intrinsic increased stiffness making it more difficult to follow the deformation of the substrate. Their behaviour is more like a separate entity. They undergo brittle fracture and delamination with large initial spalling (subsurface initiated fatigue) when submitted to cyclic loading and unloading. At high Hertzian pressures, they are even exfoliated from the rolling contact surfaces. However, as demonstrated by *Erdemir et al.*[20] under milder contact stresses where plastic deformation of the underlying substrate is minimal, thicker coatings can also improve the fatigue lifetime.

At this point, it should be recalled that the coatings investigated in this chapter are mainly aimed for cutting tool applications, where a thicker coating is favourable. It has been shown that even when a thicker coating is locally worn through, the remaining coating still protects the substrate and is capable of carrying the full load of the chip without collapsing.[21] Consequently, the present study examines the rolling contact fatigue mechanisms, which are considered to be independent of the coating thickness, rather than the influence of coating thickness on the establishment of fatigue life charts.

6.5.2 MECHANISMS OF DAMAGE

Registration of the vibration level combined with visual inspection during testing was used to monitor the growth rate of fatigue damage. Figure 6.9a and 6.9b shows the vibration level *versus* the contact cycle for TiN and TiN/(Ti,Al)N multilayers deposited onto high speed steel, respectively. For both systems,

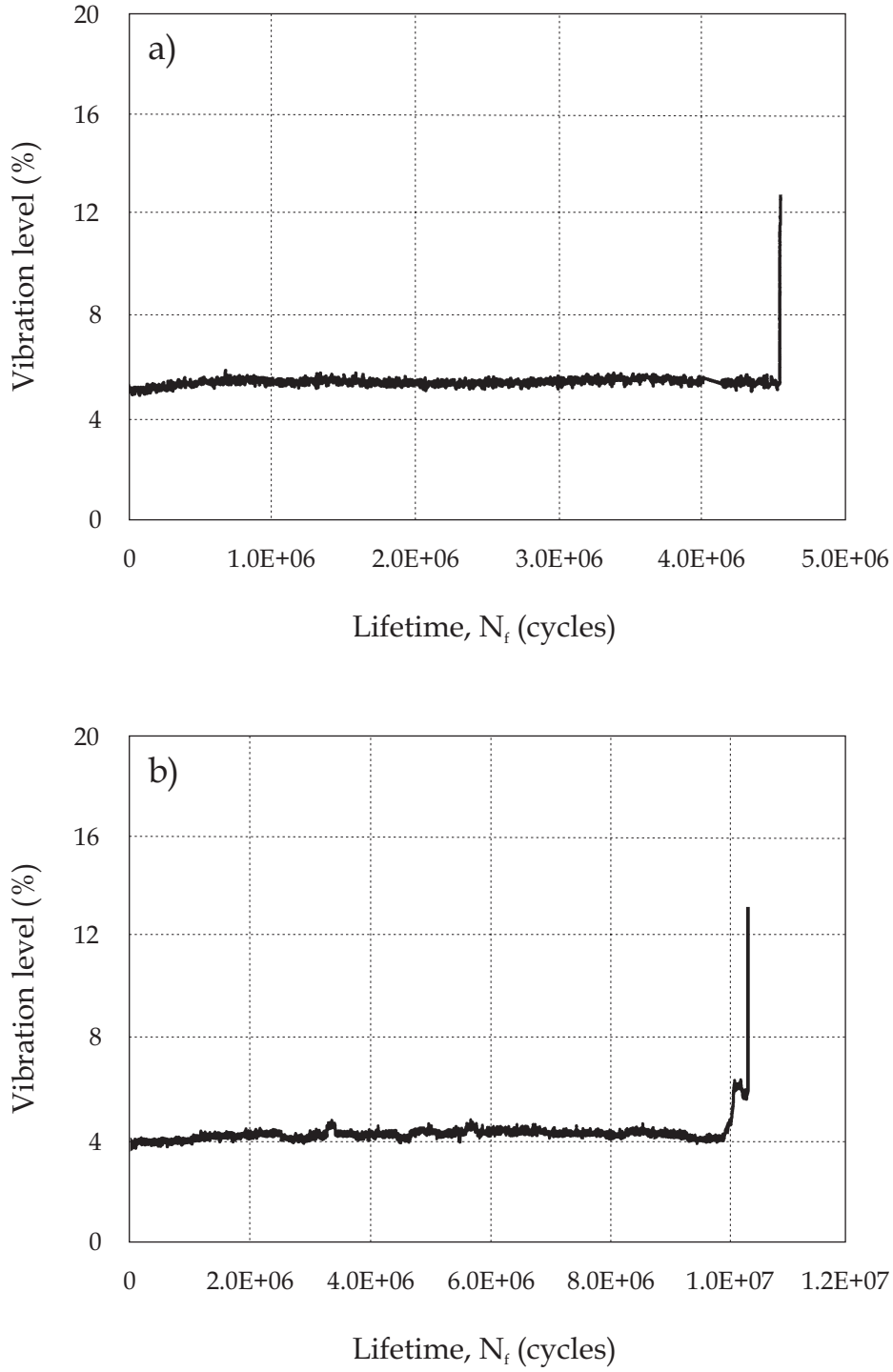

Figure 6.9 *Registered vibration level versus rolling contact cycles of* (a) *TiN and* (b) *TiN/(Ti,Al)N multilayers deposited onto high speed steel substrates. A vibration level in the range of 15% to 20% corresponds roughly to 1% delamination of the rolling contact.*

there is an incubation period without any detectable surface damage, followed by a fast growth to failure which appears to terminate the life of the coated system. This stress cycle can be used to define the fatigue life of the specific system. It was observed that at the end of the incubation time, the coating presented a relatively small patch (typical 50 μm long) and a damaged area grew from it in the rolling direction by chipping removal. By continuing rolling, some of the delaminated sites were united leading to millimetre long damage patches. Figure 6.10 illustrates the worn surfaces of various coated systems.

The failure mode of coated system with a substrate of 50 HRc is different from the others. In this case, the failure is characterised by damage of the coating spanning over the entire track width (about 1 mm) that expose the substrate. Cracks are running in the rolling direction and fracture has occurred around the contact area. The cracks occur due to tensile stresses generated when the soft substrate plastically deforms and piles-up at the rolling track edges.

When the homogeneous and multilayer coatings are deposited onto harder substrates, their failure is initiated after an incubation time. Small patches of damaged coating appeared. As the patches grow with contact cycle, the surface inside the damage patches becomes rougher due to exposed substrate and to extensive bowing of cracks in the rolling direction. To gain a deeper insight into the nature of the damage that occurs under cyclic rolling contact conditions, the damage patches were cross-sectioned. The cross-sectional SEM micrograph of figure 6.11a shows the typical failure of TiN coatings onto the softer substrate. As hinted before, the failure of hard coating-soft substrate system is not caused by conventional wear of the rolling contact, but by fracture of the coating normal to the surface and substrate fracture due to plastic deformation. Upon increasing the substrate hardness, cracks are generally initiated at the interface and propagate in the coating parallel to the surface. When the subsurface cracks branch off towards the surface, a small piece of material is released, resulting in spalling failure, as can be seen in figure 6.11b. The process of crack initiation and growth can be explained using the model developed by *Otsuka et al.*[22] The first stage of damage is the formation of fine mode II cracks parallel to the contact surface which are created by the cyclic shear component of the contact stress. The cracks occur at interfacial regions where flaws might exist due to mismatch of lattice constants and thermal expansion constants between the

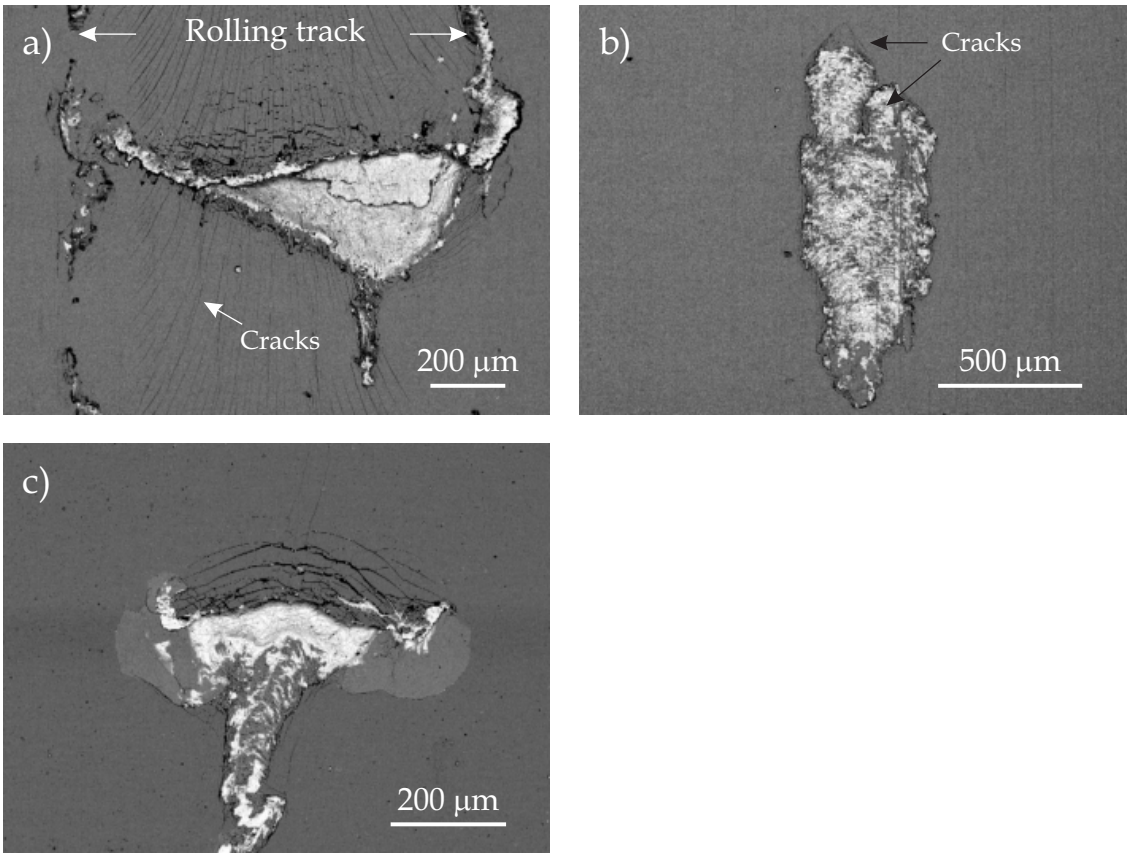

Figure 6.10 *SEM micrographs showing the worn contact surfaces of various coated systems. The micrographs were obtained with a backscattered electron detector. As the backscattered intensity increases with atomic number, the bright areas in the micrographs correspond to the steel substrate.* (a) *TiN deposited onto a substrate of 50 HRc.* (b) *TiN and* (c) *TiN/(Ti,Al)N multilayers, both deposited onto a substrate of 60 HRc. The rolling direction for all coated systems is from bottom to top.*

coating and the substrate. The next stage consists of fast growth of the initial fine cracks into macroscopic cracks both by extension of themselves and by coalescence with neighbouring cracks as stress cycling continues. The outcome is a surface distress spalling fatigue failure along these extended cracks.

The observations suggest that the interfacial bonding strength controls the fatigue behaviour under cyclic loading and unloading. Therefore, the shear strength at the interface region is increased when the mechanical bonding is improved. These results are in agreement with the analysis with contact

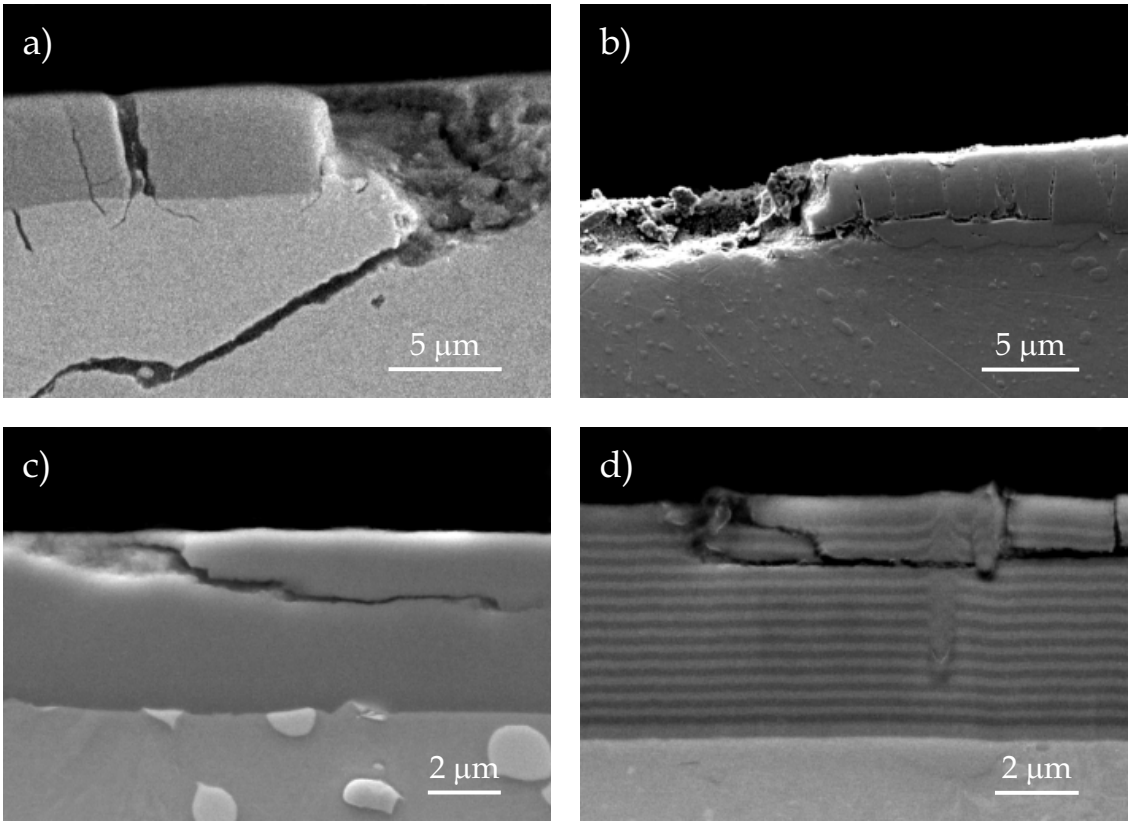

Figure 6.11 *Cross-sectional SEM micrographs exhibiting the failure modes of the coated system:* (a) *and* (b) *are of the TiN deposited onto cold work steel substrate of 50 HRc and 60 HRc, respectively;* (c) *is of the TiN deposited onto high speed steel of 67 HRc;* (d) *is of the TiN/(Ti,Al)N multilayers deposited onto cold work steel of 67 HRc.*

mechanics, showing that the shear stress range $\Delta\tau_{zx}$ at the interface is the appropriate parameter that should be used to characterise interfacial failure and cyclic bonding strength of hard coatings.[5]

Coated systems with high speed steel substrate have an equivalent failure mechanism. Nevertheless, as the fatigue lifetime is increased, small damage patches are produced by localised exfoliation. This is created by cracks propagating approximately parallel to the surface within the coating (cohesive failure), as shown in figure 6.11c. The multilayer coated system failure mechanism is presented in figure 6.11d. The SEM micrograph is from a system having a cold work steel substrate with 60 HRc. Thus, comparing figure 6.11d

with figure 6.11b, it is clear that the coatings exhibit a similar fatigue failure mechanism.

6.6 CONCLUSIONS

In this chapter the mechanical properties of homogeneous TiN and TiN/(Ti,Al)N multilayers have been evaluated by nanoindentation and rolling contact fatigue tests. The main conclusions are the following:

- Two regimes of crack propagation were found in the microindentation experiments. The transition depends of the indentation depth rather than on the load applied;
- The hardness and Young's modulus of TiN and TiN/(Ti,Al)N multilayers are estimated using the continuous stiffness option provided with the nanoindenter. The hardness is 31 ± 1 GPa for both coatings, whereas the Young's modulus of the former is ~500 GPa and of the latter is ~480 GPa;
- Bare substrates were submitted to rolling contact fatigue tests under the same applied load as the coated ones and no pitting or spalling of the bulk materials had occurred. Therefore this experimental method seems to be reliable for the determination of the cyclic bond strength of coated systems;
- Considerable disparity in fatigue durability is found among systems with different substrate surface finishing and roughness. Therefore, the dependence of rolling contact fatigue on the pre-treatment and surface roughness has been revealed. A finer polished surface is associated with longer lifetime;
- The major failure mode of coated systems under the present testing conditions is initiated at the interface region indicating that the fatigue lifetime is very sensitive to the interfacial bonding strength;
- In the present study the lifetime of coated system with 60 HRc is longer than with the 50 HRc substrate. The coated system can only improve the lifetime in rolling contact if the substrate is hard enough to carry the load. Otherwise, plastic or elastic deformation will take place in the substrate

under the contact and failure of the coated system occurs by fracture both in the coating and substrate;

- The failure mechanism of the TiN/(Ti,Al)N multilayers is similar to the one of the homogeneous TiN.

References

1. R. Buhl, H.K. Pulker, E. Moll, Thin Solid Films **80**, 265 (1981).
2. R.L. Hatschek, Am. Mach. Special Report **752**, 129 (1983).
3. W.C. Oliver, G.M. Pharr, J. Mater. Res. **7**, 1564 (1989).
4. J.C. Knight, T.F. Page, I.M. Hutchings, Surf. Engineering **5**, 213 (1989).
5. J.-W. He, B.C. Hendrix, N.-S. Hu, Surf. Engineering **12**, 49 (1996).
6. J.-L. Loubet, B.N. Lucas, W.C. Oliver, Mat. Res. Soc. Symp. Proc. **436**, 233 (1996).
7. S.J. Bull, E.H. Yoffe, T.F. Page, Philos. Mag. Lett. **59**, 281 (1989).
8. T.F. Page, S.V. Hainsworth, Surf. Coatings Technol. **61**, 213 (1993).
9. A.J. Whitehead, T.F. Page, Thin Solid Films **220**, 277 (1992).
10. T.F. Page, J.C. Knight, Surf. Coatings Technol. **39-40**, 339 (1989).
11. P.M. Ramsey, H.W. Chandler, T.F. Page, Surf. Coatings Technol. **49**, 504 (1991).
12. E. Török, A.J. Perry, L. Chollet, W.D. Sproul, Thin Solid Films **153**, 37 (1987).
13. T.F. Page, G.M. Pharr, J.C. Hay, W.C. Oliver, B.N. Lucas, E. Hierbert, L. Riester, Mat. Res. Soc. Symp. Proc. **522**, 53 (1998).
14. K.N. Andersen, E.J. Bienk, K.O. Schweitz. H. Reitz, J. Chevallier, P. Kringhoj, J. Bottiger, Surf. Coatings Technol. **123**, 219 (2000).
15. P. Hedenquist, M. Jacobson, S. Söderberg, Surf. Coatings Technol. **41**, 31 (1990).
16. T. Merriman, J. Kannel, J. Tribology **111**, 87 (1989).
17. A. Erdemir, Surf. Coatings Tecnhol. **54-55**, 482 (1992).
18. S.H. Kim, I.M. Keer, H.S. Cheng, Tribology Transactions **33**, 53 (1990).
19. T.-S.P. Chang, H.S. Cheng, Surf. Coatings Technol. **43-44**, 699 (1990).
20. A. Erdemir, R.F. Hochman, Surf. Coatings Technol. **36**, 755 (1988).
21. P. Hedenquist, M. Olsson, P. Wallén, Å. Kassman, S. Hogmark, M. Jacobson, Surf. Coatings Technol. **41**, 243 (1990).
22. A. Otsuka, H. Sugawara, M. Shomura, Fatigue Fract. Eng. Mater. Struct. **19**, 1265 (1996).